ORIGINAL ARTICLE

Characteristics and kinetic analysis of the catalytic pyrolysis of oily sludge under new nickel-ore–based catalysts

Jiayu Xu[1] · Longyuan Yang[2] · Hui Xu[3] · Yue Jiang[3] · Yuan Guo[3] · Shuai Ran[3] · Ying Gao[3]

Abstract

Thermal analysis of oily sludge (OS) from steel mills was conducted to understand its added value. The effect of additional catalysts (calcined olivine (C-OL), iddingsite (C-ID), xiuyan jade (C-XY), and their nickel carrier on OS pyrolysis performance was also investigated. The physical properties of OS showed a large number of resins and irons. It was found that OS pyrolysis involves water evaporation, light hydrocarbon escape, the crack of resins, asphaltene decomposition, and inorganic mineral decomposition. TG results demonstrated that the prepared catalyst can effectively improve the weight loss, in which the C-OL (Ni) increased by 11.58 wt.%. The kinetic behavior of the three main weight loss zones in the catalytic pyrolysis of OS was subsequently analyzed. The apparent activation energies of the main stages of OS pyrolysis were 61.03, 18.07, and 62.92 kJ/mol, respectively. The addition of C-OL significantly reduced the apparent activation energies by 31.34, 5.74, and 44.46 kJ/mol. The evaluation of the pre-exponential factor revealed that all stages of OS pyrolysis followed a diffusion model, and the reaction path was not changed by the ore catalysts.

Keywords Oily sludge · Nickle-based catalyst · Catalytic pyrolysis · Kinetics · Fitting method

1 Introduction

Disposal of oily sludge (OS) from industrial residues is raising more and more concerns, due to its rapidly increasing amount and potential risk [1]. In China, OS is included in the national hazardous waste list [2]. Generally, OS is considered to be derived from the petroleum extraction and refining industry, and it is a hazardous solid waste with recycling value generated in the process of mining, storage, transportation, and processing [3]. But there are also risks of dealing with OS in other industries, and these industries are often overlooked, such as OS from steel mills.

Jiayu Xu and Longyuan Yang contributed equally to this work.

✉ Hui Xu
xuhui@njtech.edu.cn

1   School of Mechanical and Power Engineering, Nanjing Tech University, Nanjing 211816, China

2   School of Environmental Science and Engineering, Hubei Polytechnic University, Huangshi 435003, China

3   School of Energy Science and Engineering, Nanjing Tech University, Nanjing 211816, China

OS is a complex, high-viscosity, semi-fluid residue, including aged crude oil, wax, resin, asphaltene, and more sediment [4]. Undoubtedly, incineration of OS has advantages such as reduction of sludge volume, destruction of organic pollutants, and energy recovery. Nevertheless, incineration has always been restricted by exhaust emissions [5, 6]. In contrast, pyrolysis can effectively avoid secondary pollution caused by flue gas [7]. Not only that, the pyrolysis reaction is more thorough, less harmful, and economical [8–10]. Collectively, pyrolysis technology has great potential for resource utilization of OS.

Some scholars tried to improve the pyrolysis performance of OS by using different additives. Lin et al. [11] pointed out that the participation of rice husk was beneficial to increasing the contents of saturates and aromatics in the pyrolysis oil. Alkali/alkaline metals are also of concern [12–14]. It has been certified that KOH could decline the concentration of asphaltenes with more saturated hydrocarbon formation [15]. Furthermore, the catalyst is also an important factor influencing the pyrolysis behavior of OS [16–18]. Gong et al. [19] found ferric oxide can accelerate the pyrolysis process and shorten the reaction time. The lattice oxygen in the ferric oxide can induce the cracking reaction of heavy components to generate light oil and carbon dioxide. Currently, natural ore has

been widely used to prepare catalysts due to its unique structure and composition [18, 20–22]. Ma et al. [23] studied the catalytic effects of dolomite and olivine on the co-gasification of coal and biomass, and they found that two natural ores had a positive influence on tar reforming. It is worth noting that loading nickel on the ore can improve its catalytic performance. Tursun et al. [24] found that NiO/olivine exhibited good in situ catalytic activity for the gasification of pine sawdust. Ni catalysts were reputed to improve hydrogen yield and minimize coke formation [25]. It must be mentioned that more researches have concentrated on the effect of catalysts on product regulation and tar reforming. The influence of ore catalysts on pyrolysis kinetic behaviors has rarely been proposed.

Thermogravimetric analysis (TGA) is a necessary technique for the study of thermal decomposition kinetic behavior [26]. According to the TGA analysis, the kinetic triplet, including the apparent activation energy (E_a), the pre-exponential factor (A), and the reaction model ($f(a)$), can be further determined by different methods [27–30]. Undeniably, the whole kinetic triplet has advantages in explaining reaction rate changes or reaction control factors [31]. It can also be said that these data may help identify the role of the ore catalysts in the mass transfer behavior of OS pyrolysis. Moreover, it can also provide important information for process parameter optimization, new pyrolysis reactor design, and targeted catalyst synthesis.

Although various noteworthy studies on OS were reported, there was no data to determine the pyrolysis reaction kinetics of OS from steel mills. Trego et al. [32] reported the pyrolysis kinetic parameters of heavy crude oil that can be regarded as "precursors" of OS. But there are differences between heavy crude oil and OS from steel mills. In addition, no relevant researches on the kinetic behaviors of the catalytic pyrolysis of OS by ores were reported. In our previous works [20, 21], calcined olivine, iddingsite, and xiuyan jade (C-OL, C-ID, and C-XY) were first confirmed to be an appropriate load platform. Subsequently, the C-OL (Ni), C-ID (Ni), and C-XY (Ni) prepared by impregnation exhibited good pyrolysis catalytic activity to OS. In this paper, the effects of these mentioned catalysts on the pyrolysis properties of OS were analyzed. Afterwards, mathematical fitting methods were adapted to evaluate the kinetic behavior of the main stages of the OS pyrolysis process. The study aims to provide kinetic data for the realization of high-efficiency and low-cost catalytic pyrolysis of OS.

2 Materials and methods

2.1 Materials

The OS sample used in this experiment was taken from the Baoshan Iron & Steel Co., Ltd., Shanghai. The large

impurities in the samples were manually screened. Then the samples were pre-dried in a vacuum drying oven at 105 ℃ for 12 h. Proximate and ultimate analyses were measured according to the Chinese GB/T 212–2008 and GB/T 476–2001. Saturates, aromatics, resins, and asphaltenes (SARA) analysis of OS extract was conducted using the Chinese standard SY/T 5119–2008, and ICP analysis was carried out via Agilent ICP-OES 730. All the results are shown in Table 1. It is obvious that OS from steel mills was rich in Fe. Compared with the OS in Ref. [15], this OS contains more resins and lower saturates and aromatics.

In this paper, three natural ore catalysts, OL, ID, and XY, were purchased from Xinjiang Province, China. The same pre-treatment method as in Ref. [20] was adopted to obtain C-OL, C-ID, and C-XY. The catalysts were crushed and sieved to 60 mesh to attain suitable catalyst carriers. The catalysts were calcined at 900 ℃ under an air atmosphere for 4 h. Afterwards, the impregnation method was utilized to load Ni on the ore surfaces. The details were introduced in Ref. [21]. The calcined catalysts were added to the nickel chloride solution (1.96 wt.%) and stirred mechanically for 12 h, and then the obtained precipitates were dried at 105 ℃ overnight and calcined at 900 ℃. The final obtained catalysts were denoted as C-OL (Ni), C-ID (Ni), and C-XY (Ni), respectively.

2.2 Experimental methods

The pyrolysis experiments were performed by non-isothermal thermogravimetry in a thermogravimetric analyzer model STA449-F1 (TA Instruments, manufactured in Germany). Before the thermogravimetric experiments, the OS and the catalysts were blended in a ratio of 5:2. In each experiment, 10 ± 0.5 mg of sample was added into a crucible, followed by heating from room temperature up to 900 ℃

Table 1 The proximate analysis, ultimate analysis, SARA analysis, and ICP-OES analysis of the OS sample

Proximate analysis [ad] (wt.%)		Ultimate analysis (wt.%)	
Moisture	27.87	C	16.75
Volatile	28.38	H	2.21
Ash	36.10	N	0.27
Fixed carbon	7.65	S	0.25
		O	18.27
SARA analysis (wt.%)		ICP-OES (mg/g)	
Saturates	14.17	Fe	129.8
Aromatics	8.22	Zn	2.27
Resins	74.28	Ni	0.11
Asphaltenes	3.34	Pb	0.17

ad air-dried basis

with a heating rate of 5 ℃/min in the nitrogen atmosphere. The gas flow rate was 100 mL/min.

2.3 Kinetic calculation

For variations in chemical components of OS, the entire pyrolysis reaction mechanism cannot be accurately predicted. But a popular formula [33] can be used to describe the overall reaction mechanism,

$$\text{Oilysludge (Solid Waste)} \xrightarrow{k(T)} \text{Volatile (Gas + Tar) + Char(Solid residue)} \quad (1)$$
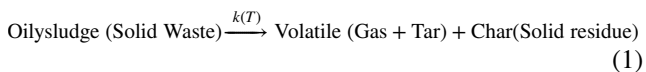
This formula can be adapted for different pyrolysis stages. We approximate each stage as the only single-step one. Hence, the rate constant of reaction (k) can be given by the Arrhenius equation: $k = Aexp\left(-\frac{E}{RT}\right)$ Here, k is the reaction rate constant, A is the pre-exponential factor (min^{-1}), E_α is the apparent activation energy (kJ/mol), R is the gas constant (8.314 J/(mol·K)), and T is the absolute temperature (K). The reaction rate ($d\alpha/dt$) of pyrolysis of the OS is a linear function of rate constant and reaction kinetic model ($f(\alpha)$), and can be written as:

$$\frac{d\alpha}{dt} = k \cdot f(\alpha) \quad (2)$$

where α is the conversion rate of sample, which can be calculated by the following equation:

$$\alpha = \frac{(m_0 - m_t)}{(m_0 - m_f)} \quad (3)$$

where m_0 is the initial weight of the sample, m_t is the mass of sample at time t, and m_f is the mass of the sample at the end of the pyrolysis reaction. By substituting the Arrhenius equation into Eq. (2), we get,

$$\frac{d\alpha}{dt} = Af(\alpha)exp\left(-\frac{E}{RT}\right) \quad (4)$$

For non-isothermal experiments, the temperature is a linear function of time, and the slope is the heating rate, which is a constant, described as $\beta = dT/dt$. Thus, Eq. (5) and Eq. (6) can be obtained,

$$\frac{d\alpha}{dT} = \frac{A}{\beta}f(\alpha)exp\left(-\frac{E}{RT}\right) \quad (5)$$

$$g(\alpha) = \int_0^\alpha \frac{da}{f(a)} = \frac{A}{\beta}\int_{T_0}^T exp\left(-\frac{E}{RT}\right)dT = \frac{AE}{\beta R}p(x) \quad (6)$$

Equation (6) is the integral form of the reaction model and $x = \frac{E}{RT}$ The temperature integral ($p(x)$) has no exact analytical solution; therefore, an approximate integral formula can be used instead [34],

$$1n\left[\frac{g(\alpha)}{T^2}\right] = 1n\left(\frac{AE}{\beta R}\right) - \frac{E}{RT} \quad (7)$$

The common reaction mechanism models in integral form are shown in Table 2. Kinetic plot between $1n\left[\frac{g(\alpha)}{T^2}\right]$ versus $\frac{1}{T}$ will give slope and intercepts used for calculation of apparent activation energy E and pre-exponential factor A.

3 Results and discussion

3.1 Pyrolysis behavior of OS

Figure 1 represents the TG and DTG profiles of the OS pyrolysis at 5 ℃/min from the room temperature to 900 ℃. There are five stages in the pyrolysis process, which is similar to the point in Ref. [19], and the peaks representing each stage have been marked on the DTG curve. The first stage is water evaporation, which occurred up to the temperature of 140 ℃. The mass loss recorded at this stage is 0.956 wt.%. The maximum weight loss rate in this stage was 0.0422%/min, which appeared at 64 ℃. The weight loss in this stage is not obvious, which was attributed to the pre-drying of the samples. The second and third stages were inseparable. In the range of 140 to 345 ℃, the slope of the TG curve is stable. However, the DTG curve showed that this cannot be seen as a single stage. There was a shoulder between 140 and 270 ℃, determined as the second stage. The weight loss in the second stage was 8.161 wt.%. This stage was represented by the DTG peak that reached the maximum at 254.29 ℃, where the highest weight loss rate of this stage was 0.55%/min. The shoulder was related to the priority of light components escape, such as saturates with small molecular mass. The third stage was observed between 270 and 345 ℃ where the weight loss is 8.854 wt.%. The weight loss rate of the third stage of OS pyrolysis was even higher than that of the second stage, indicating the continuation of the light components escape. The maximum DTG peak was recorded at 299 ℃ with a weight loss rate of 0.745%/min, which can be attributed predominantly to the simultaneous crack of heavy components. Specifically, the resin was related to this stage because it contained a large number of labile alkyl chains, which were cracked from 200 ℃ [32]. This phenomenon would continue until the resins were completely converted to coke. The temperature interval of the fourth stage started at 345 ℃ and ended at 510 ℃, where a weight loss of 9.516 wt.% took place. The maximum weight loss rate of this stage was 0.402%/min at 434 ℃. The weight loss of the fourth stage was mainly linked to partial carbon decomposition.

Table 2 The common kinetic models in integral form for solid-state reactions [35]

Model	Mechanism	$g(\alpha)$
Nucleation models		
P2	Power law	$\alpha^{1/2}$
P3	Power law	$\alpha^{1/3}$
P4	Power law	$\alpha^{1/4}$
P2/3	Power law	$\alpha^{3/2}$
A2	Avrami-Erofeev	$[-1n(1-\alpha)]^{1/2}$
A3	Avrami-Erofeev	$[-1n(1-\alpha)]^{1/3}$
A4	Avrami-Erofeev	$[-1n(1-\alpha)]^{1/4}$
Reaction order models		
F1	First order reaction	$-1n(1-\alpha)$
F2	Second order reaction	$-1n(1-\alpha)^{-1}-1$
F3	Third order reaction	$(1/2)[(1-\alpha)^{-2}-1]$
Geometrical contraction models		
R2	Contracting cylinder	$1-(1-\alpha)^{1/2}$
R3	Contracting cylinder	$1-(1-\alpha)^{1/3}$
Diffusion models		
D1	One-dimensional diffusion	α^2
D2	Two-dimensional diffusion	$(1-\alpha)1n(1-\alpha)+\alpha$
D3	Three-dimensional diffusion	$[1-(1-\alpha^{1/3})]^2$
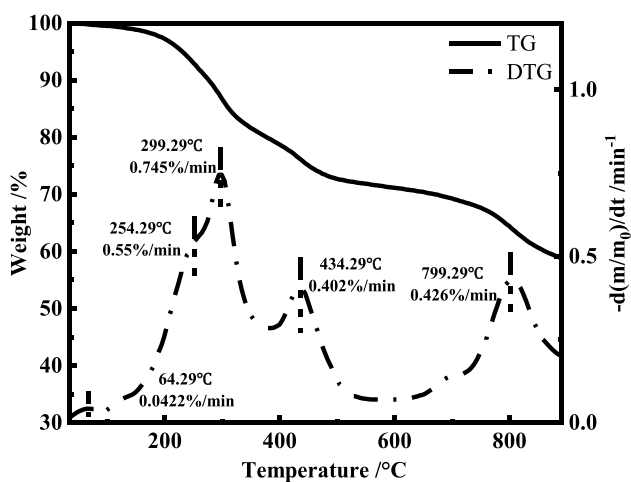
Fig. 1 TG and DTG curves of OS

In detail, the cracking and polycondensation of asphaltenes were the main theme of this stage. Additionally, the resin was also converted into coke through asphaltenes. The significant weight loss rates at a temperature above 730 ℃ indicated the beginning of a new stage, defined as the fifth stage. The fifth stage continued up to 900 ℃ with a weight loss of 9.745 wt.%. The maximum weight loss rate in this stage was read as 0.426%/min at 799 ℃. The weight loss of this stage can be associated with the decomposition of inorganic minerals. The final residue amount at the end of pyrolysis was 58.653 wt.%, which is significantly greater than the ash

content determined by the industrial analysis, which means that there was still more coke remaining in the residue.

3.2 Pyrolysis behavior of OS with catalysts

Figure 2a and b illustrate the TG and DTG curves of OS with C-OL and C-OL (Ni) recorded from room temperature to 900 ℃ at a heating rate of 5 ℃/min. Figure 2a presents that the catalysts could effectively inhibit the production of residue. The addition of C-OL and C-OL (Ni) dropped the final residue to 56.79 wt.% and 47.49 wt.%, respectively. Compared with C-OL, the nickel-based catalyst had better performance. It can be seen from Fig. 2b that the maximum weight loss rate of pyrolysis blending with catalysts appeared in advance. The DTG curves demonstrated that the maximum weight loss of pyrolysis with catalysts at the second and third stages was higher than without. However, in the fourth stage, the catalysts reversely promoted carbon decomposition represented by the lower weight loss rates of 0.347%/min and 0.361%/min, respectively. In the last stage, C-OL (Ni) performed significantly for the weight loss rate of 0.575%/min, indicating that nickel could disrupt the process of asphaltene polycondensation to provide more small molecules.

TG and DTG curves of the OS mixed with C-ID and C-ID (Ni) are displayed in Fig. 2c and d. It can be observed from Fig. 2c that C-ID and C-ID (Ni) can also reduce the amount of pyrolysis residues. The pyrolysis residues involved in C-ID and C-ID (Ni) were 56.79 wt.% and 49.52 wt.%,

Fig. 2 TG and DTG curves of OS with different catalysts. (**a**) and (**b**) C-OL/C-OL (Ni); (**c**) and (**d**) C-ID/C-ID (Ni); (**e**) and (**f**) C-XY/C-XY (Ni)
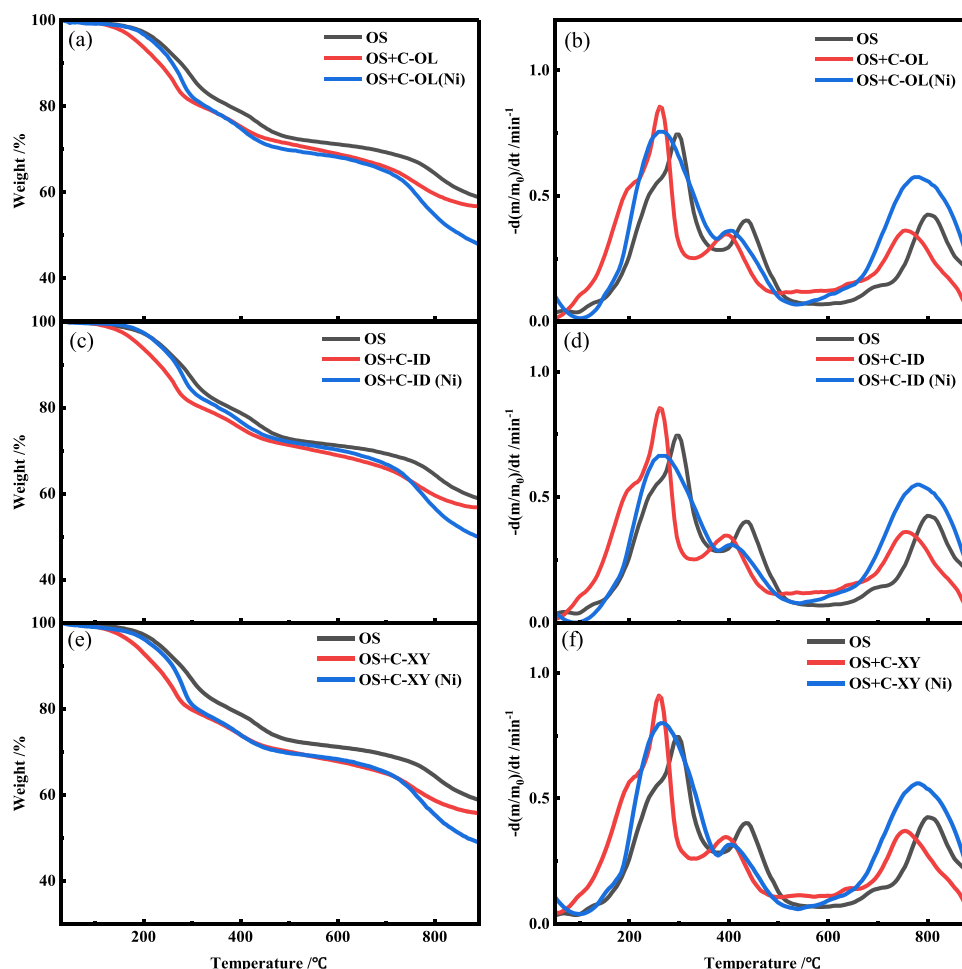
respectively. Figure 2d shows that the DTG curve of C-ID in the second and third stages shifted to low temperature and had a higher rate of weight loss, revealing that it preferentially promoted the escape of light components and the crack of heavy components. But in the later stages, C-ID did not perform a good catalytic effect as a lower maximum weight loss rate in the DTG curve. C-ID (Ni) had a clear advantage in the final stage for the fast-declining TG curve and the high maximum weight loss rate of 0.55%/min. However, in the range of 160 to 510 ℃, the maximum weight loss rate of pyrolysis with C-ID (Ni) is relatively low, only 0.665%/min and 0.31%/min at 263 ℃ and 403 ℃, respectively.

Figure 2e and f have displayed the TG and DTG curves of OS blending with C-XY and C-XY (Ni). XY-derived catalysts presented a similar performance to the others mentioned in this study in reducing pyrolysis residues. With the participation of C-XY (Ni), there was 48.603 wt.% of pyrolysis residues. The DTG curves viewed in Fig. 2f demonstrated that the temperature corresponding to the maximum weight loss rate shifted to left in all stages. In the range of 160 to 345 ℃, the maximum weightless peak of OS with C-XY was recorded as 0.91%/min, which is higher than that

of OS with C-XY (Ni) observed as 0.8%/min. The maximum weight loss rates of C-XY and C-XY (Ni) were 0.347%/min and 0.316%/min at 394.19 ℃ and 403.27℃, respectively. In the final area, the weightless peak of pyrolysis of the OS with C-XY (Ni) arrived at 0.56%/min, while that of pyrolysis of the OS with C-XY was 0.362%/min, which is below 0.426%/min represented by without additives.

In general, the catalysts have a significant impact on the pyrolysis process of OS, whether it is loaded with Ni or not, and the Ni-loaded ones are mainly responsible for the changes in the pyrolysis characteristics of the OS in the high-temperature section.

3.3 Kinetic analysis of OS pyrolysis with different catalysts

The main reactions of OS pyrolysis appeared at 140–510 ℃ and 700–900 ℃, which corresponded to stage 2, stage 3, stage 4, and stage 5. The stage was a rough division of the reaction mechanism, which was not suitable to represent the kinetic model. In the OS pyrolysis, the escape of light components and the crack of heavy components were

simultaneous behaviors according to the DTG curve. Therefore, from the perspective of the kinetic model, an attempt to build a model that includes stage 2 and stage 3 was appropriate. A simplified kinetic model is a necessary method for kinetic analysis. Figure 3 presents the kinetic curves of the main reaction stages of OS pyrolysis calculated by fitting models. The kinetic parameters of the apparent activation energies (E_a), correlation coefficients (R^2), and frequency factors (A) of OS pyrolysis are illustrated in Table 3. Stage 2/3 was defined as the combination of stage 2 and stage 3. It is clear that the reaction mechanisms of the three stages all follow the diffusion model (the stage 2/3 and stage 4 follow D2, stage 5 follows D3), and the correlation coefficients of the stages are all above 0.90, denoting a good fitting effect. The fitting apparent activation energies of all stages were 61.03, 18.07, and 62.92 kJ/mol, respectively. The apparent energy is usually used to estimate the difficulty of the reaction, which represents the lowest effective energy required to break down the chemical bonds. The E of the stage 2/3 was recorded as a higher value. This may be attributed to the cleavage of heavy components consuming more energy. The apparent activation energy of the stage 4 was much lower than the others. In general, resins disrupted the π–π and polar bonding interactions between asphaltene monomers, which results in asphaltenes being broken with low energy [36, 37]. The stage 5 expanded the most energy, which was associated with the complex interaction of coke and ash residues [38]. Iron and its oxides were the most abundant components in the ash residues. In the OS, the iron content was observed as high as 129.8 mg/g, and iron ions were more easily formed, which subsequently attracted nitrogen, sulfur, and polar oxygen functional groups in asphaltenes through coordination bonds, causing the formation of coke, were adsorbed on the ash residues through coordination. The break of this bond costs more energy. To deduce an insight into the reaction chemistry of the pyrolysis of OS, the order magnitude of the pre-exponential factor is a useful reference [39]. The pre-exponential factors of the all stages were 543.78, 0.029, and 10.07 min^{-1}, respectively. In the case of an order of magnitude lower than 10^9 min^{-1}, the surface reaction is the working pathway [35, 39, 40].

Table 4 shows the fitting parameters of the main reaction stages of OS pyrolysis with catalysts. The kinetic curves of all samples are illustrated in the Appendix. It is demonstrated that some curves fitted well with the reaction order models (R^2 was higher than 0.9). But in fact, these curves also had a similar degree of fit to diffusion models. It is virtually impossible to conclude that the catalysts had changed the reaction mechanism of OS pyrolysis based on the value of R^2. In general, the catalysts could lower the total apparent activation energy of OS, except for C-ID (Ni). The E of stages 2/3, 4, and 5 decreased from 61.03, 18.07, and 62.92 kJ/mol to 29.69, 12.33, and 18.46 kJ/mol with
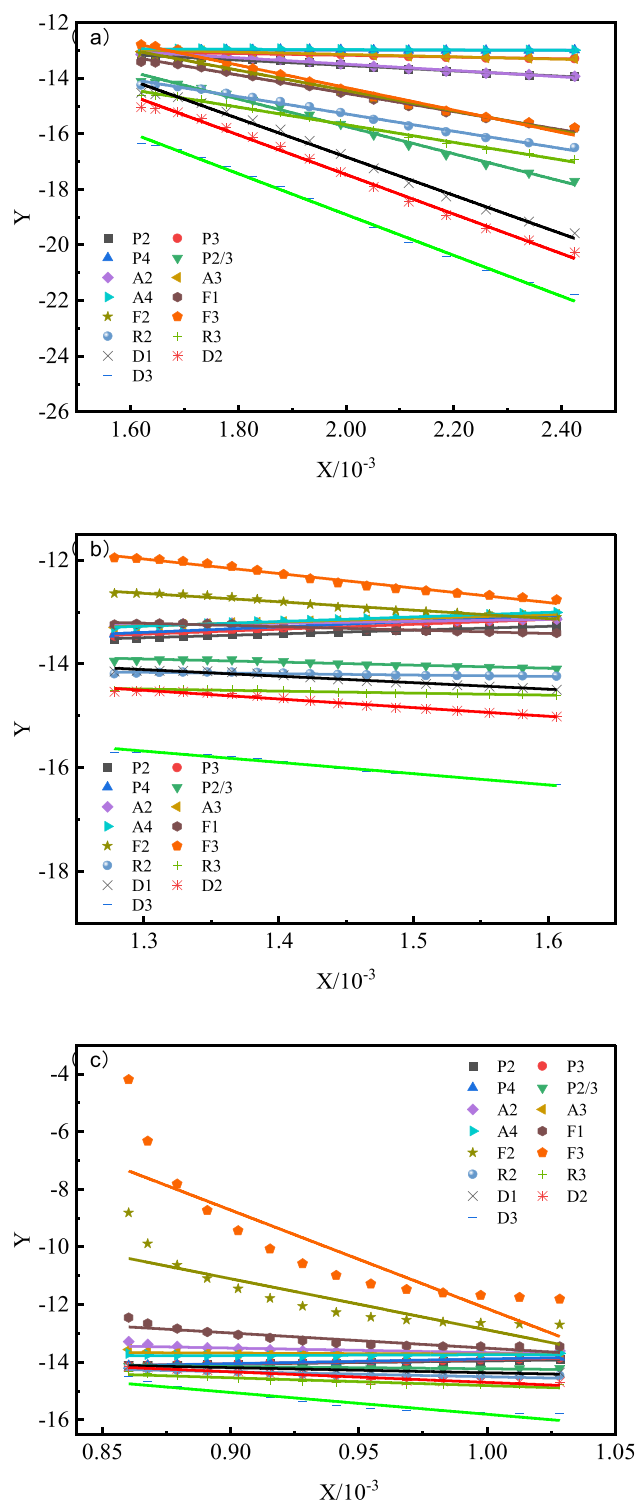
Fig. 3 The kinetic curves of the main reaction stages of OS pyrolysis: (**a**) stage 2/3, (**b**) stage 4, (**c**) stage 5

the addition of C-OL, respectively. Its performance was conspicuous. But when nickel was loaded on C-OL, the E change was not obvious, especially in stage 2/3, which only dropped by 4.21 kJ/mol. The same performance also

Table 3 Fitting parameters of the main reaction stages of OS pyrolysis

Stage	Reaction model	E (kJ·mol^{-1})	A (min^{-1})	R^2
Stage 2/3	D3	61.03	543.78	0.99547
Stage 4	D3	18.07	0.029	0.98372
Stage 5	D2	62.92	10.07	0.93785

Table 4 Fitting parameters of the main reaction stages of OS pyrolysis with catalysts

	Stage	Reaction model	E (kJ·mol^{-1})	A (min^{-1})	R^2
OS/C-OL	Stage 2/3	F2	29.69	4.75	0.99927
	Stage 4	D3	12.33	0.009	0.98782
	Stage 5	D2	18.46	0.0566	0.92117
OS/C-OL (Ni)	Stage 2/3	D3	56.82	174.49	0.97537
	Stage 4	F2	14.52	44.58	0.92054
	Stage 5	D2	37.5	0.76	0.96034
OS/C-ID	Stage 2/3	F3	32.15	56.43	0.99871
	Stage 4	F3	16.67	0.97	0.97883
	Stage 5	D2	24.84	0.16	0.98615
OS/C-ID (Ni)	Stage 2/3	D3	65.83	1148	0.98043
	Stage 4	F3	13.99	0.28	0.95079
	Stage 5	D2	69.50	21.57	0.96222
OS/C-XY	Stage 2/3	F2	26.83	12.42	0.99852
	Stage 4	F3	16.21	0.96	0.97429
	Stage 5	D2	20.81	0.083	0.96467
OS/C-XY (Ni)	Stage 2/3	D1	53.72	829.27	0.97708
	Stage 4	F3	12.58	0.24	0.95931
	Stage 5	D2	36.66	0.69	0.96129

appeared in C-ID (Ni) and C-XY (Ni). In the case of C-ID (Ni) participation, the apparent activation energy increased to 65.83 kJ/mol instead. The change of apparent activation energy is closely related to the reaction model. For the diffusion model, the apparent activation energy is positively correlated with the change of the heat and mass diffusion. In other words, for a reaction dominated by a diffusion model, the reaction rate is determined by the heat and mass diffusion rather than the chemical reaction. The ore catalysts had a well-developed pore structure, which was beneficial to the diffusion of light components during the reaction. Nonetheless, when nickel chloride was loaded, part of the pore structure may be blocked, causing the catalyst's mass transfer performance to be weakened. Therefore, it can be seen that nickel chloride has the greatest restriction on C-ID. It can also be explained that the apparent activation energy of stage 5 loaded with nickel chloride is higher than that without loading. Consequently, it implied that the catalyst did not

change the pyrolysis reaction model of OS, and it was still a diffusion model. The addition of C-OL reduced the apparent activation energy of stages 2/3, 4, and 5 to 32.15, 16.67, and 24.84 kJ/mol, respectively. Furthermore, C-XY dropped the apparent activation energy of the three stages to 26.83, 16.21, and 20.81 kJ/mol, respectively. From the perspective of apparent activation energy, C-OL, C-ID, and C-XY had a similar catalytic performance for OS; however, after loading nickel, C-XY(Ni) was prior to the others, which was consistent with experimental results [21]. The addition of catalysts did not significantly change the order of magnitude of the pre-exponential factor of OS pyrolysis (all A were lower than 10^9 min^{-1}), which indicated that the reaction still took the surface reaction as the path.

4 Conclusion

In this work, the non-catalytic and catalytic pyrolysis using natural ore catalysts of OS were investigated by thermogravimetric analysis. The results showed that the OS pyrolysis can be divided into five stages: water evaporation, light hydrocarbon escape, the crack of resins (heavy components), asphaltene decomposition, and inorganic mineral decomposition.

On the TG/DTG curves, the selected natural ores did not show obvious differences. The addition of catalysts reduced the mass fraction of OS pyrolysis residue and caused the DTG curves to shift to the left. The ore carriers had a positive effect on the cracking of heavy components in the OS, which was manifested in the prominent DTG peak. The participation of nickel had a significant effect on the formation and decomposition of coke during the pyrolysis of OS.

From the perspective of kinetic analysis, OS pyrolysis mainly included stage 2/3, stage 4, and stage 5, and their apparent activation energies were 61.03, 18.07, and 62.92 kJ/mol, respectively. The magnitude of the pre-exponential factor indicated that OS pyrolysis was a surface reaction. The catalysts could effectively reduce the apparent activation energy of OS pyrolysis. C-OL had the best performance, with apparent activation energies reduced to 29.69, 12.33, and 18.46 kJ/mol, respectively. Consistently, the pyrolysis reaction path of OS was not changed by the catalysts. The study unveils for the first time the kinetic parameters of the pyrolysis of OS from steel mills under nickel-ore–based catalysts, which provides a new perspective for the treatment of OS from steel mills.

Declarations

Competing interests The authors declare no competing interests.

References

1. Jin X, Teng D, Fang J et al (2021) Petroleum oil and products recovery from oily sludge: characterization and analysis of pyrolysis products. Environ Res 202:111675. https://doi.org/10.1016/j.envres.2021.111675

2. Zhang L, Tong K, Wang X et al (2015) Research progress of ultrasonic technology for oil sludge treatment. Environ Protect Oil Gas Fields (in Chinese) 25:73-76+87

3. Song Q, Zhao H, Jia J et al (2019) Characterization of the products obtained by pyrolysis of oil sludge with steel slag in a continuous pyrolysis-magnetic separation reactor. Fuel 255:115711. https://doi.org/10.1016/j.fuel.2019.115711

4. Huang Q, Han X, Mao F et al (2014) A model for predicting solid particle behavior in petroleum sludge during centrifugation. Fuel 117:95–102. https://doi.org/10.1016/j.fuel.2013.09.002

5. Karamalidis AK, Voudrias EA (2007) Release of Zn, Ni, Cu, SO_4^{2-} and CrO_4^{2-} as a function of pH from cement-based stabilized/solidified refinery oily sludge and ash from incineration of oily sludge. J Hazardous Mater 141:591–606. https://doi.org/10.1016/j.jhazmat.2006.07.034

6. Wang Z, Guo Q, Liu X, Cao C (2007) Low temperature pyrolysis characteristics of oil sludge under various heating conditions. Energy Fuels 21:957–962. https://doi.org/10.1021/ef060628g

7. Gao N, Li J, Quan C, Tan H (2020) Product property and environmental risk assessment of heavy metals during pyrolysis of oily sludge with fly ash additive. Fuel 266:117090. https://doi.org/10.1016/j.fuel.2020.117090

8. Kan T, Strezov V, Evans TJ (2016) Lignocellulosic biomass pyrolysis: a review of product properties and effects of pyrolysis parameters. Renew Sustain Energy Rev 57:1126–1140. https://doi.org/10.1016/j.rser.2015.12.185

9. Fahmy TYA, Fahmy Y, Mobarak F et al (2020) Biomass pyrolysis: past, present, and future. Environ Dev Sustain 22:17–32. https://doi.org/10.1007/s10668-018-0200-5

10. Hu X, Gholizadeh M (2019) Biomass pyrolysis: a review of the process development and challenges from initial researches up to the commercialisation stage. J Energy Chem 39:109–143. https://doi.org/10.1016/j.jechem.2019.01.024

11. Lin B, Huang Q, Chi Y (2018) Co-pyrolysis of oily sludge and rice husk for improving pyrolysis oil quality. Fuel Processing Technol 177:275–282. https://doi.org/10.1016/j.fuproc.2018.05.002

12. S C, Y W, N G, et al (2016) Pyrolysis of oil sludge with oil sludge ash additive employing a stirred tank reactor. Journal of Analytical and Applied Pyrolysis 120:511 520 https://doi.org/10.1016/j.jaap.2016.06.024

13. Shie J-L, Lin J-P, Chang C-Y et al (2003) Pyrolysis of oil sludge with additives of sodium and potassium compounds. Resour Conserv Recycl 39:51–64. https://doi.org/10.1016/S0921-3449(02)00120-9

14. Heng Q, Huang S, Lou W et al (2021) Study on the difference between in-situ and ex-situ catalytic pyrolysis of oily sludge. Environ Sci Pollut Res 28:50500–50509. https://doi.org/10.1007/s11356-021-14233-6

15. Lin B, Wang J, Huang Q, Chi Y (2017) Effects of potassium hydroxide on the catalytic pyrolysis of oily sludge for high-quality oil product. Fuel 200:124–133. https://doi.org/10.1016/j.fuel.2017.03.065

16. Hou J, Zhong D, Liu W (2022) Catalytic co-pyrolysis of oil sludge and biomass over ZSM-5 for production of aromatic platform chemicals. Chemosphere 291:132912. https://doi.org/10.1016/j.chemosphere.2021.132912

17. Wang F, Zhang H, Du M et al (2021) Effects of TiO_2/bentonite on the pyrolysis process of oily sludge. Nat Environ Pollut Technol 20:1–12

18. Wang Q, Hao K, Benally C et al (2022) The role and potential of attapulgite in catalytic pyrolysis of refinery waste activated sludge. Pet Sci 19:354–362. https://doi.org/10.1016/j.petsci.2021.09.043

19. Gong Z, Zhang H, Liu C et al (2021) Co-pyrolysis characteristics and kinetic analysis of oil sludge with different additives. J Therm Sci 30:1452–1467. https://doi.org/10.1007/s11630-021-1421-8

20. Lu C, Zhang X, Gao Y et al (2021) Parametric study of catalytic co-gasification of cotton stalk and aqueous phase from wheat straw using hydrothermal carbonation. Energy 216:119266. https://doi.org/10.1016/j.energy.2020.119266

21. Zhang X, Xu J, Ran S et al (2022) Experimental study on catalytic pyrolysis of oily sludge for H_2 production under new nickel-ore-based catalysts. Energy 249:123675. https://doi.org/10.1016/j.energy.2022.123675

22. Yang J, Xu X, Liang S et al (2018) Enhanced hydrogen production in catalytic pyrolysis of sewage sludge by red mud: thermogravimetric kinetic analysis and pyrolysis characteristics. Int J Hydrog Energy 43:7795–7807. https://doi.org/10.1016/j.ijhydene.2018.03.018

23. Ma X, Zhao X, Gu J, Shi J (2019) Co-gasification of coal and biomass blends using dolomite and olivine as catalysts. Renew Energy 132:509–514. https://doi.org/10.1016/j.renene.2018.07.077

24. Tursun Y, Xu S, Abulikemu A, Dilinuer T (2019) Biomass gasification for hydrogen rich gas in a decoupled triple bed gasifier with olivine and NiO/olivine. Bioresour Technol 272:241–248

25. Yao D, Yang H, Chen H, Williams PT (2018) Investigation of nickel-impregnated zeolite catalysts for hydrogen/syngas production from the catalytic reforming of waste polyethylene. Appl Catal B 227:477–487. https://doi.org/10.1016/j.apcatb.2018.01.050

26. Vyazovkin S (2002) Thermal analysis. Anal Chem 74:2749–2762. https://doi.org/10.1021/ac020219r

27. Pinzi S, Buratti C, Bartocci P et al (2020) A simplified method for kinetic modeling of coffee silver skin pyrolysis by coupling pseudo-components peaks deconvolution analysis and model free-isoconversional methods. Fuel 278:118260. https://doi.org/10.1016/j.fuel.2020.118260

28. Mishra RK, Mohanty K (2018) Pyrolysis kinetics and thermal behavior of waste sawdust biomass using thermogravimetric analysis. Bioresour Technol 251:63–74. https://doi.org/10.1016/j.biortech.2017.12.029

29. Mian I, Li X, Jian Y et al (2019) Kinetic study of biomass pellet pyrolysis by using distributed activation energy model and Coats Redfern methods and their comparison. Bioresour Technol 294:122099. https://doi.org/10.1016/j.biortech.2019.122099

30. Subramanian S, Ragula UBR (2020) Kinetics of catalytic and non-catalytic pyrolysis of Nerium oleander. Fuel 280:118591. https://doi.org/10.1016/j.fuel.2020.118591

31. Vyazovkin S, Burnham AK, Favergeon L et al (2020) ICTAC Kinetics Committee recommendations for analysis of multi-step kinetics. Thermochimica Acta 689:178597. https://doi.org/10.1016/j.tca.2020.178597

32. Trejo F, Rana MS, Ancheyta J (2010) Thermogravimetric determination of coke from asphaltenes, resins and sediments and coking kinetics of heavy crude asphaltenes. Catalysis Today 150:272–278. https://doi.org/10.1016/j.cattod.2009.07.091

33. Sadhukhan AK, Gupta P, Saha RK (2009) Modelling of pyrolysis of large wood particles. Bioresour Technol 100:3134–3139. https://doi.org/10.1016/j.biortech.2009.01.007

34. Coats AW, Redfern JP (1964) Kinetic parameters from thermogravimetric data. Nature 201:68–69. https://doi.org/10.1038/201068a0

35. Alves JLF, da Silva JCG, Mumbach GD et al (2022) Prospection of catole coconut (Syagrus cearensis) as a new bioenergy feedstock: insights from physicochemical characterization, pyrolysis kinetics, and thermodynamics parameters. Renew Energy 181:207–218. https://doi.org/10.1016/j.renene.2021.09.053

36. Spiecker PM, Gawrys KL, Trail CB, Kilpatrick PK (2003) Effects of petroleum resins on asphaltene aggregation and water-in-oil emulsion formation. Colloids Surf A: Physicochem and Eng Aspects 220:9–27. https://doi.org/10.1016/S0927-7757(03)00079-7

37. Moncayo-Riascos I, Taborda E, Hoyos BA et al (2020) Effect of resin/asphaltene ratio on the rheological behavior of asphaltene solutions in a de-asphalted oil and p-xylene: a theoretical–experimental approach. J Mol Liq 315:113754. https://doi.org/10.1016/j.molliq.2020.113754

38. Schorling P-C, Kessel DG, Rahimian I (1999) Influence of the crude oil resin/asphaltene ratio on the stability of oil/water emulsions. Colloids Surf A: Physicochem Eng Aspects 152:95–102. https://doi.org/10.1016/S0927-7757(98)00686-4

39. Gupta GK, Mondal MK (2019) Kinetics and thermodynamic analysis of maize cob pyrolysis for its bioenergy potential using thermogravimetric analyzer. J Therm Anal Calorim 137:1431–1441. https://doi.org/10.1007/s10973-019-08053-7

40. Badshah SL, Shah Z, Alves JLF et al (2021) Kinetic and thermodynamics study of the pyrolytic process of the freshwater macroalga, Chara vulgaris. J Appl Phycol 33:2511–2521. https://doi.org/10.1007/s10811-021-02459-3